Robust Adaptive Supervisory Fractional Order Controller for Optimal Energy Management in Wind Turbine with Battery Storage

B. Meghni, D. Dib, Ahmad Taher Azar, S. Ghoudelbourk
and A. Saadoun

Abstract To address the challenges of poor grid stability, intermittency of wind speed, lack of decision-making, and low economic benefits, many countries have set strict grid codes that wind power generators must accomplish. One of the major factors that can increase the efficiency of wind turbines (WTs) is the simultaneous control of the different parts in several operating area. A high performance controller can significantly increase the amount and quality of energy that can be captured from wind. The main problem associated with control design in wind generator is the presence of asymmetric in the dynamic model of the system, which makes a generic supervisory control scheme for the power management of WT complicated. Consequently, supervisory controller can be utilized as the main building block of a wind farm controller (offshore), which meets the grid code requirements and can increased the efficiency of WTs, the stability and intermit-

B. Meghni
Faculty of Applied Science, Department of Electrical Engineering,
University of KasdiMerbah, 3000 Ouargla, Algeria
e-mail: maghni_1990@yahoo.fr

D. Dib · S. Ghoudelbourk
Department of Electrical Engineering, University Larbi Tebessi,
Tébessa, Algeria
e-mail: dibdjalel@gmail.com

S. Ghoudelbourk
e-mail: sghoudelbourk@yahoo.fr

A.T. Azar (✉)
Faculty of Computers and Information, Benha University,
AlQalyubiyah, Banha, Egypt
e-mail: ahmad_t_azar@ieee.org; ahmad.azar@fci.bu.edu.eg

A.T. Azar
Nanoelectronics Integrated Systems Center (NISC),
Nile University, Cairo, Egypt

A. Saadoun
Department of Electronics, University of Badji Mokhtar,
Annaba, Algeria
e-mail: saadoun_a@yahoo.fr

tency problems of wind power generation. This Chapter proposes a new robust adaptive supervisory controller for the optimal management of a variable speed turbines (VST) and a battery energy storage system (BESS) in both regions (II and III) simultaneously under wind speed variation and grid demand changes. To this end, the second order sliding mode (SOSMC) with the adaptive gain super-twisting control law and fuzzy logic control (FLC) are used in the machine side, BESS side and grid side converters. The control objectives are fourfold:

  (i)   Control of the rotor speed to track the optimal value;
 (ii)   Maximum Power Point Tracking (MPPT) mode or power limit mode for adaptive control;
(iii)   Maintain the DC bus voltage close to its nominal value;
(iv)   Ensure: a smooth regulation of grid active and reactive power quantity, a satisfactory power factor correction and a high harmonic performance in relation to the AC source and eliminating the chattering effect.

Results of extensive simulation studies prove that the proposed supervisory control system guarantees to track reference signals with a high harmonic performance despite external disturbance uncertainties.

Keywords Power management · A high performance · Supervisory control · Wind turbine · Fuzzy logic · Second order sliding mode control, power limit

1   Introduction

Because of the environmental problems, the oil crisis and the growing demand for energy, wind energy is one of the most mature of the different renewable energy technologies which received a lot of concern and attention in perceptible many parts of the world [1].

   Nowadays, specifically related to offshore wind turbines, wind conversion technology showed new aspects of its construction and operation. Current WT operate at variable speed based PMSG and without speed multiplier, this type of wind turbines increase energy efficiency, reduce mechanical stress, can work with a high power factor and improve the quality of the electrical energy produced by WT compared to fixed speed [2].

   For this type (VSWT), doubly fed induction generator (DFIG) and permanent magnet synchronous generators PMSGs are the most used technologies [3]. Today, due to its simple structure with characteristic self-excitation that can work with: a good performance, high reliability, good performance control and a great capacity for maximizing the power extracting by the MPPT, the PMSG topology is required, it is recommended to be connected to the variable speed wind turbines (VSWTs) [4]. Moreover, this technology is better in the case of offshore wind, as maintenance is simpler and less expensive compared to a technology using a gearbox.
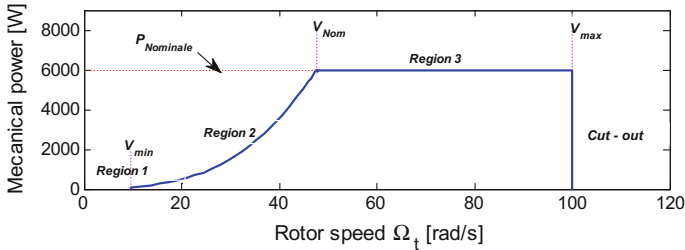
Fig. 1 Operation regions for VSWT

Practically and for safety reasons turbines and uniform stability between supply and demand of energy, wind turbines work only in a specified range of wind speeds limited by $(v\,cut - in)$ and $(v\,cut - out)$ as is shown in Fig. 1, where the possibility of three different operating zones [5].

- Region 1: when the wind speed is below the speed $(V\,cut - in)$ wind, no maximize efficiency that occurs in this region.
- Region 2: when the wind speed exceeds $(V\,cut - in)$ but under the rated $(Vnom)$. In this area the main controller is to increase the efficiency of the power extracted from the WTs, so it operates at its maximum power point (MPP).
- Region 3: when the wind speed is greater than $(Vnom)$ but under the $cut - out$ wind speed $(Vmax)$; the task of the controller is to keep the power captured at a fixed or nominal value instead of trying to maximize it. Another important controller objective in this last region, is to keep the electrical and structural conditions in a safety region [5, 6].

Despite this characteristic, the utmost challenge of wind power generation is the inherently sporadic nature of the wind which can deviate quickly. Its intermittent availability is the main impediment to power quality and flow control. Therefore, the stability and power quality of the grid operation is affected. Consequently, the fluctuations of wind power should be reduced to prevent a degradation of the grid's performance [7].

In the new universal grid code for wind power generation, the power oscillation damping by wind energy is included. For instance, the energy storage system (ESS) is integrated with the renewable sources which are connected into the power grid to maintain the safe operation of the power grid, balance the supply and demand sides, and enhance fault ride-through ability and damp short-term power oscillation [8]. There are different types of ESSs in the power systems such as batteries ESS, superconducting magnetic ESS, compressed air, hydrogen ESS, gravitational potential energy with water reservoirs, electric double layer capacitor, and flywheels [9]. The BESS is one of the most rapid growing storage technologies. The BESS installation cost and generating noise are relatively lower than the other storage technologies.

However, these features remain restricted with respect to the practical domain of variation of wind speed. Therefore, effective architecture of control systems are one

of the major issues in hybrid VSWT (managing variations in load demand and to extract maximum power) to prevent possible degradation on the quality of electrical energy delivered into the electric grid, where variations of the loads and generations are significant in the system.

This goal has been and is a motivation for researchers and investors to search on robust and effective control strategies for VSWT to overcome various constraints such as the optimal tracking point controller has been developed in many literatures especially for wind energy systems [5], to track the maximum wind power available at each instant. They include namely, tip speed ratio (TSR) [5], sliding mode control (SMC) [10], the hill-climb searching (HCS) [5] and fuzzy logic control (FLC) [11] techniques. Several methods of power limitation control and pitch power control have been advanced in some studies [12–14]. Effective techniques have been developed in many papers to control the optimal rotational speed of the wind turbine in order to determine the maximum power coefficient for a given wind speed. Some of these variable speed techniques are FOSMC [15], SOSMC [16] and FLC [17], robust control [18]. Numerous recent studies [9] advanced the benefit of the energy storage techniques to mitigate the unpredictable character of wind energies, ensuring more efficient management of the available resources and provide operation freedom to wind generation that allows time-shifting between generation and demand. More robust and efficient strategies based on modern control techniques such as fuzzy logic control [19], robust control [20] and sliding mode control [21] have been widely developed and implemented to smooth regulation of the grid active and reactive powers exchanges between the PMSG and the grid.

1.1 Contribution of the Paper

Based on our previous research experience on WT/battery hybrid power system and their supervisory control system [22], a key contribution of this study is to present a comprehensive model of the proposed structure based on WT/battery hybrid power system and to implement **the novel supervisory control system in order to optimize the power output and protecting all the system.** This proposed management strategy is achieved through the combination of the efficient and robust control methods described in recent publications in order to develop a perfect wind system.

Furthermore, contrary to the works found in the literature, this work presents a new approach to control and management for extended Control & of VSWT that includes simultaneously the two **operating regions (II and III)** whatever the speed variation the wind. This adaptation **(commutation of control system in both regions)** may provide better performance in all possible operational scenarios of the wind: extract the maximum power from the wind, storage of excess power, compensation of power between supply and demand, limiting the upper power at nominal generator or demand.

For this reason (To reach this goal), the control objectives are three in number; the first on the generator side converter, the second on bidirectional DC/DC converter and the last one on the grid side converter.

1. The main function of the generator side controller is to track the maximum power via speed loop control based on SOSMC. An MPPT control algorithm, based on an FLC, has been used to regulate the rotational speed in order to tack accurately the PMSG working point to its maximum power point (MPP) and to derive the rotational speed reference. (Force the working point of the PMSG to its MPP and to provide the rotational speed reference). In the case studied in control subsystem, two adaptive and commutative operation modes are distinguished:

   - When the aerodynamic power is not enough to reach the synchronous speed, the system operates at mode 1(tracking mode MPPT): maximum power extraction, whereas, if the wind speed exceeds the rated value, the system switches to mode 2 (Power Limitation mode): power limitation, which leads the PMSG to provide its rated power below nominal speed of the rotor.

2. A bidirectional DC/DC converter is connected between the battery and the DC bus. This converter is controlled to maintain the DC bus voltage at its rated value, allowing the active power, bi-directional active power flow from the battery, through the charge/discharge of the device in response to the variations of the operating conditions (regardless of the variations of the operating conditions).
3. In the grid side converter, a SOSMC controller has been used to achieve smooth regulation of active and reactive power quantities exchange between the BESS and the grid according to grid demand under real fluctuating wind speed (region II and III).

1.2 Organization of the Research Work

The paper is organized as follows. In Sect. 2, are view of the previous related work is presented. In Sect. 3, the modeling of the PMSG wind turbine and ESS is described. Section 4 presents in detail the proposed supervisory control applied in this work. The simulations results and robustness test are illustrated in Sect. 5. Finally, the conclusions of the obtained results and future work are shown in Sect. 6.

2 Related Work

Much research has been do in recent years to improve system performance monitoring and management of the energy produced by the WTs where several techniques have been proposed various structures of WT, such as artificial neural

networks (ANN) [23–25], FLC [26–28], the first order sliding mode [15, 29, 30] and the SOSMC [31–33]. The main reason for this interest is that these techniques and structures were used to achieve a new and robust optimization that actually works for VSWT problems that cannot be solved by conventional techniques. Similarly, recent contributions remained within certain limits due to multiple ignored or neglected issues such as MPPT, power control, power limit, speed control and energy storage system. These problems contribute to the degradation of the performance of WTs.

In Ref. [34], a PSIM software integration study was performed in more than one MPPT used FLC technique where the results are limited, because the study is applied to as simple structure without a storage system, security system in rated wind speed and without power control for the grid side.

Moreover, in the second part of the study by [35], the authors proposed a technique based on the strategy FOSMC to control the active and reactive power injected to the grid. The simulation results show a poor power quality produced in the presence of the chattering phenomenon.

Furthermore, the reference [3] shows an original method for the sensorless MPPT of a small power wind turbine using a permanent magnet synchronous generator (PMSG). On the other hand the operating range of this system is limited in the region 2, because it not contains any limit power control or pitch control in rated wind speed.

On [9, 36–38] the authors treated with details, modeling and control of a hybrid system composed of DFIG/WT and ESS. The results are convincing, but the authors have not applied effective and robust control techniques in key points such as MPPT, speed control, power control of the grid, which makes these reliable studies only normal and stable working conditions (wind speed constant, no default in the wind channel and no fault in the grid).Also In these studies the authors adopted only on the operating area 2 (This is what makes activity limited by WT).

The advanced control algorithms FLC and SOMSC were proposed by [11] to simulate VSWT-based DFIG. Although the results were attractive, choosing the type of machine used remains not determinant. Further- more, the authors assessed a method of limiting the power extracted from a gust of wind, while they have ignored the use of storage means to earn excess wind power. In the Refs. [39–42], the authors have developed MPPT techniques to optimize the performance of the power extracted from the wind in (region II). These contributions have given a great success in this field. These studies are not considered to be a perfect solution unless we can successfully integrate advanced techniques for power management to consumption (power control). Other hand, when the demand for power exceeds the power extracted, the MPPT technology will not be able to satisfy the demand; hence, the need for a compensation system ESS.

In reference [22] the authors generally succeed in the choice of the supervisory control system which applied in hybrid VSWT. But they are neglect the protection of the wind system (electric and mechanic) under the rated wind speed in addition they are limiting the operating range of wind turbine.

Despite the amazing results presented in the previous studies, these remains limited and insufficient to face various restrictions (because these control strategies are usually used separately for each type of study to VSWT). The new supervisory control system proposed in WTs has become a solution necessary for the optimal management of the electric and mechanical power in any part of the wind channel. This new system is based on the combination in the same type WT of new algorithms (robust, effective and flexible) to work in various areas simultaneously (Region II and III) with high precision, which makes it universal for different types of WT.

3 Dynamic Model of PMSG-WT

In this section the studied system is presented. In order to achieve the system control and a first study by simulation before implementation, its modelling is required. Figure 2 shows a representative topology of the investigated wind energy system. As illustrated in this figure the offshore VSWT a horizontal axis turbine with a three-bladed rotor design directly transmits the aerodynamic torque and power to PMSG (without a gearbox). The generator power is then fed to the utility grid by means of power electronic devices (two back-to-back IGBT bridges AC/DC/AC) interconnected by a common DC bus. This WT is supported by an ESS associated with DC bus system composed of a lead acid battery with a bidirectional DC/DC converter.

3.1 Wind Turbine Aerodynamic

For a variable speed wind turbine, the mechanical power and torque extracts from the wind turbine is proportional to the wind speed and can be calculated by the following formulas [10]:
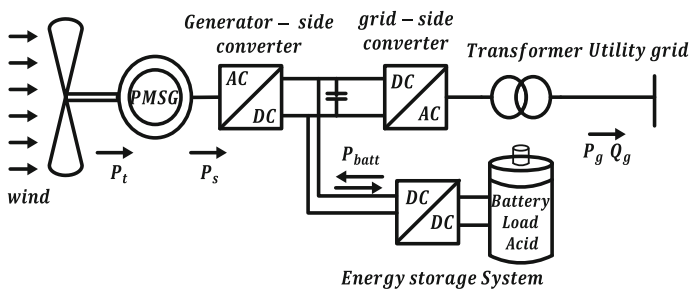

Fig. 2 Wind generation system configuration

$$P_t = \frac{1}{2}\rho\pi R_t^2 v^3 C_p(\lambda,\beta) \tag{1}$$

$$T_t = \frac{P_t}{\Omega_t} = \frac{1}{2\lambda}\rho\pi R_t^3 v^2 C_p(\lambda,\beta) \tag{2}$$

Which λ present the ratio between the wind speed and the turbine angular speed. This ratio is called tip speed ration:

$$\lambda = \frac{R_t \Omega_t}{v} \tag{3}$$

where: λ is the tip speed ratio, C_p is the power coefficient, β is the pitch angle, Ω_t is the rotor speed (rad/s), R_t is the rotor-planeradius (m), ρ is the air density (Kg/m^3).

The coefficient C_p is a variable magnitude as a function of λ, the theoretically possible maximum value of the power is β. The C_p is different for each wind turbine, as shown in [43]. Theoretically, the Betz limit is ≈ 0.5926 further and practically, friction and the force dragged reduce this value to 0.5 for large wind turbines [44]. Calculating another analytic expression $C_p(\lambda)$ for different values of β is also possible.

For a pitch angle β given, the analytical expression commonly used is a polynomial regression as follows [45]:

$$C_p = 0.073\left(\frac{151}{\lambda_i} - 0.058\beta - 0.002\beta^{2.14} - 13.2\right)e^{\frac{-18.4}{\lambda_i}} \tag{4}$$

Where $\lambda_i = \frac{1}{\frac{1}{\lambda - 0.02,\beta} - \frac{0.003}{\beta^2 + 1}}$

The aerodynamic characteristics of a variable speed turbine are usually represented by the relationship $C_p(\lambda)$ as illustrated in Fig. 3.
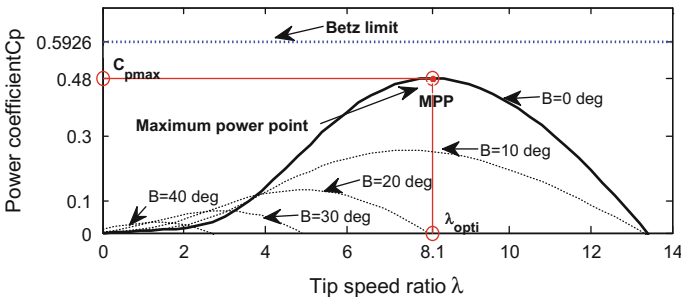

Fig. 3 Typical C_p versus λ curve

From this figure and according to Eqs. (1, 3), we can conclude that for a fixed value of $\beta = 0$, C_p only becomes a nonlinear function of λ. According to Eq. (3), there is a relationship between λ and Ω_t and at some, power is maximized at some Ω_t optimal speed Ω_{topti}. This rate corresponds to a λ_{opti}. The value of λ is constant for all the maximum power point (MPP) [5].

Thus, to extract maximum power at wind speeds of variable λ must be adjusted to its optimum value λ_{opti} followed a maximal power coefficient value C_p, to follow the optimum operating point. From Eqs. (1, 3), we get [46]:

$$P_{tmax} = \frac{1}{2} \rho \, \pi \, R_t^5 \left(\frac{C_{p.max}}{\lambda_{opti}^3} \right) \Omega_{topti}^3 \tag{5}$$

$$\Omega_{topti} = \frac{\lambda_{opti} v}{R_t} \tag{6}$$

3.2 Model of PMSG

The simple dynamic model of three-phase PMSG in d, q reference frame can be represented by the following voltages equations [45]:

$$V_{sd} = R_s I_{sd} + L_d \frac{dI_{sd}}{dt} - \omega_e L_q I_{sq} \tag{7}$$

$$V_{sq} = R_s I_{sq} + L_q \frac{dI_{sq}}{dt} + \omega_e (L_d I_{sd} + \psi_m) \tag{8}$$

Where $V_{sd}, V_{sq}(V)$ are the direct and quadrature components of the PMSG voltages, R_s, L_d and L_q respectively are the resistance, the direct and the quadrature inductance of the PMSG winding, $\psi_m(wb)$ represents the magnet flux, $\omega_e(rad/s)$ is the electrical rotational speed of PMSG $I_{sd}, I_{sq}(A)$ are the direct and quadrature components of the PMSG currents respectively.

Now the mechanical dynamic equation of a PMSG is given by [47]:

$$\frac{d\Omega_t}{dt} = \frac{1}{J_T} T_e + \frac{D_T}{J_T} \Omega_t - \frac{1}{J_T} T_t \tag{9}$$

The electromagnetic torque of a p-pole machine is obtained as [47]:

$$T_e = \frac{3}{2} n_p (\psi_m I_{sq} + (L_d - L_q) I_{sd} I_{sq}) \tag{10}$$

Where $(N.m)$ is the electromagnetic torque, n_p is the number of pole pairs, D_T is the damping coefficient, J_T is the moment of inertia.

3.3 Model of the Grid

The dynamic model of the grid connection in reference frame rotating synchronously with the grid voltage is given as follows [10].

$$V_{dg} = V_{di} - R_g I_{dg} - L_{dg}\frac{dI_{dg}}{dt} + L_{qg}w_g I_{qg} \tag{11}$$

$$V_{qg} = V_{qi} - R_g I_{qg} - L_{qg}\frac{dI_{qg}}{dt} - L_{dg}w_g I_{dg} \tag{12}$$

The DC-link system equation can be given by:

$$C\frac{dV_{DC}}{dt} = \frac{3}{2}\frac{V_{dg}}{V_{DC}}I_{dg} - I_{DC} \tag{13}$$

Where: $V_{dg}, V_{qg}(V)$ are the direct and quadrature components of the grid voltages, $V_{di}, V_{qi}(V)$ are the inverter voltages components, (R_g, L_{dg}, L_{qg}) are resistance, the direct and quadrature grid inductance respectively, $I_{dg}, I_{qg}(A)$ are the direct and quadrature components of the grid currents respectively, V_{DC} is the DC-link voltage, I_{DC} is the grid side transmission line current and C is the DC-link capacitor.

The power equations in the synchronous reference frame are given by [34]:

$$P_g = \frac{3}{2}(V_{dg}I_{dg} + V_{qg}I_{qg}) \tag{14}$$

$$Q_g = \frac{3}{2}(V_{dg}I_{qg} - V_{qg}I_{dg}) \tag{15}$$

After orienting the reference frame along the grid voltage, V_{qg} equals to zero by aligning the d-axis. Then, the active and reactive power can be obtained in this new reference from the following equations [34]:
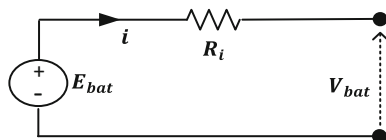
$$P_g = \frac{3}{2}V_{dg}I_{dg} \tag{16}$$

$$Q_g = \frac{3}{2}V_{dg}I_{qg} \tag{17}$$

3.4 Model of the ESS

The lead-acid battery used in this work is modeled by the battery model included in Sim Power Systems [48] where it is modeled as a variable voltage source in series

Fig. 4 Lead-acid battery simplest model [49]

with an equivalent internal resistance (see Fig. 4). The battery voltage is given by Eq. (18).

$$V_{bat} = E_{bat} - R_i i \tag{18}$$

The voltage of the rated load for the period of the charging or discharging of the battery depends on the internal battery parameters such as: the battery current, the hysteresis phenomenon of the battery during the charging and discharging cycles and the capacity extracted [36].

$$\begin{cases} E_{batdisch} = E_0 - K\frac{Q}{Q-i_t}i^* - K\frac{Q}{Q-i_t}i_t + f_{hyst-disch}(i) \\ E_{batcharg} = E_0 - K\frac{Q}{0.1Q+|i_t|}i^* - K\frac{Q}{Q-i_t}i_t + f_{hyst-char}(i) \end{cases} \tag{19}$$

Where V_{bat} is the battery rated voltage, $E_{batdisch}$ is the discharge voltage, $E_{batcharg}$ is the charge voltage, E_0 is internal EMF, R_i is internal resistance, K is the polarisation constant (V/Ah), Q is battery capacity (Ah), i_t is the actual battery charge and i^* is the filtered current.

In most electrochemical batteries, it is important to maintain the SOC within limits recommended to prevent internal damage. The instantaneous value of the load condition is calculated by [36]:

$$SOC = 1 - \frac{Q_e}{C(0,\theta)}, \ DOC = 1 - \frac{Q_e}{C(I_{avg},\theta)} \tag{20}$$

Where: SOC is battery state of charge, $Q_e(A.s)$ is the battery's charge, DOC is battery depth of charge, $I_{avg}(A)$ is the mean discharge current, $C(A.s)$ is the battery's capacity.

3.5 Battery Converter Modeling

Different converters based PWM DC/DC are used to connect the various energy sources to the DC bus, these converters are used to control the flow of energy between sources to maintain the DC bus at a constant value. In this present work, the electro-chemical battery is connected to the DC bus of PMSG through a bidirectional converter (buck-boost) DC/DC power. The structure of this converter is shown in Fig. 5. It consists of a high-frequency inductor, an output filtering capacitor, and two IGBT-diodes switches.

Fig. 5 Bidirectional DC/DC
battery power converter
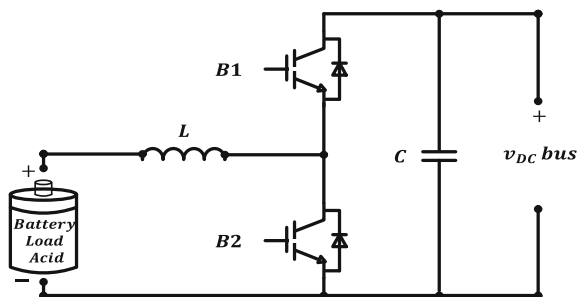
This makes it possible to charging and discharging the battery in both directions to keep the DC bus voltage to a reference value independent of variations the battery voltage. During the charging phase, the power flows from the DC link bus to the BESS through the B_1 switch and B_2 diode. Therefore, the converter can acts like a unidirectional buck converter. On another side, the battery discharges through the B_2 switch and B_1 diode, furnishing energy to the DC bus. In this period, the converter acts like a unidirectional boost converter [7].

4   Proposed Control System

The supervisory control system of hybrid WT has the responsibility to provide appropriate regulation, stability, protection, optimization and tracking objectives for the WT rotor speed in various constraints (supply and demand changing, sporadic nature of the wind, different operating region (region II or III) and the unexpected faults in the grid).

In order to achieve this goal, we have optimized our concept of classical supervisory control [22], for makes the WT operate in a wide range of wind speeds (region II and III).

The major objective most of the control systems used in this paper are:

- In Region II: Capture of maximum energy from the wind, through the combination advanced control based on FLC-SOSMC applied to machine side converter (MSC).
- In Region III: Power limitation, above the rated wind speed, this control must limit the extracted power by adaptive control (FLC-SOSMC-MPPT and the sensed extracted power as a feedback).
- In both regions (II and III): Managing energy between generated and consumed energies of the hybrid system components using the supervisory controller (through the battery side converter BSC).
- In both regions (II and III): Power quality improvement, through the robust and efficiency strategy control (SOSMC) applied in the grid side converter (GSC).

4.1 Control of the Machine Side Converter (MSC)

VSWTs are designed to achieve maximum aerodynamic effective on a wide range of wind speeds, which sometimes include several areas of operation. However, this degree of freedom requires a system of speed/sophisticated and robust power control to overcome various constraints to monitor the point of maximum available power (Region II) and to limit the power captured when the wind speed exceeds a certain par value (region III). In this section, we showed the design of the machine side controller as shown in Fig. 6. (Control side of the converter machine (MSC)) that includes two additional operating modes (adaptive).

1. **Tracking mode (Region II)**

In this area and to meet the total demand for power, the turbine operates at variable speed under a nominal wind speed between $(vcut - in)$ and $(vcut - out)$. For this reason the cascade control structure with two control loop have been created. In the outer loop, a (MPPT) algorithm based on advanced technology FLC-SOSMC is designed to permanently extract the optimal aerodynamic energy in order to generate the electromagnetic torque reference. Whereas, in the inner loop we controlled the dq-axis current of the generator according to the Eq. (8) and by field oriented control strategy (FOC) of the PMSG to ensure that the system works around the optimal point, which corresponds to the maximum power extracted by the turbine [50].

For a fixed value of $\beta = 0$ and for each wind speed, the MPPT algorithm uses fuzzy logic controller generates the reference speed that maximizes the extracted power from the turbine as shown in Fig. 7.

To ensure a quick and smooth tracking of the maximum power without the knowledge of the characteristic of the turbine and the wind speed measurement,
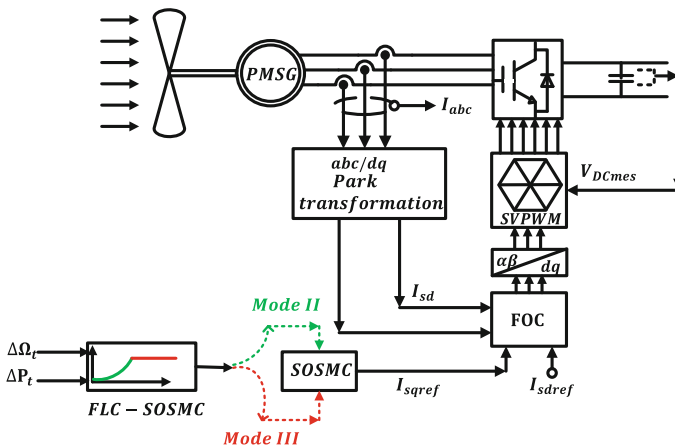

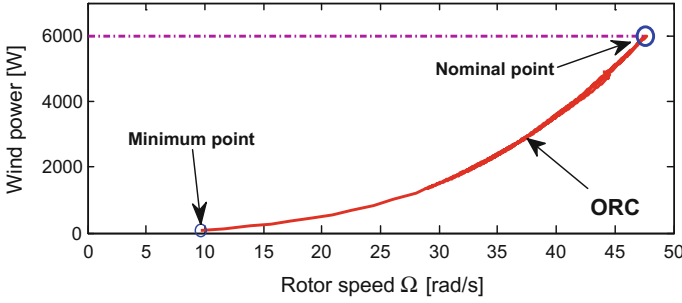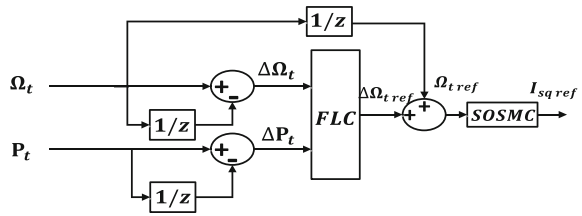**Fig. 6** Control block diagram of machine side converter

Fig. 7 Real tracking the optimal rotational speed ORC in "region II"

Fig. 8 Input and output of fuzzy controller

FLC technique is used for generating a reference speed allowing the WT run around the maximum points at varying wind speeds as shown in Fig. 8. This technique has become universal for the different types of WT [11]. The proposed fuzzy controller has two inputs and an output. The base rule of the system is given in Table 1, and the variation step in the speed reference and power is indicated in Fig. 9.

The Eq. (21) show that the relationship between the optimum speed rotation, the extracted power and wind speed are linear. For this reason, the MPPT-FLC device based on measurement of power change ΔP_t and rotational speed $\Delta \Omega_t$ propose a variation $\Delta \Omega_{tref}$ of the turbine rotational speed reference according to the following equations:

$$
\begin{cases}
\Delta P_t = P_t(k) - P_t(k-1) \\
\Delta \Omega_t = \Omega_t(k) - \Omega_t(k-1) \\
\Omega_{tref} = \Omega_t(k-1) + \Delta \Omega_{tref}
\end{cases}
\tag{21}
$$

Table 1 Rules of fuzzy logic controller

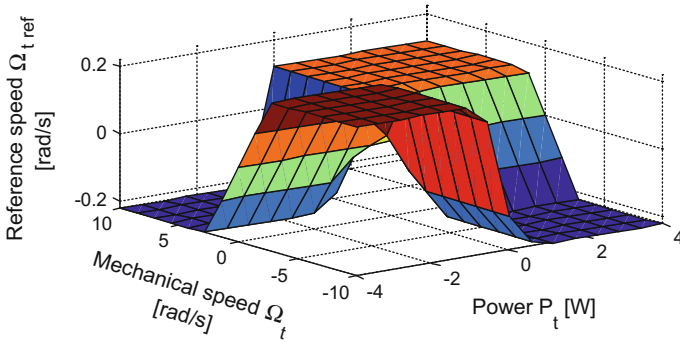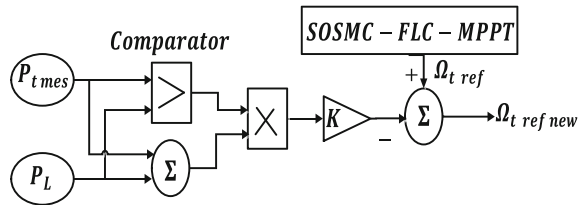| $\Delta \Omega_t$	ΔP_t								
	NBB	NB	NM	NS	ZE	PS	PM	PB	PBB
N	PBB	PB	PM	PS	ZE	NS	NM	NB	NBB
ZE	NB	NB	NM	NS	ZE	PS	PM	PB	PB
P	NBB	NM	NS	NB	ZE	PM	PM	PM	PBB

Fig. 9 Control surface of 2D fuzzy controller

Fig. 10 Detailed block
diagram of the power limit

In the same part, the reference speed (along which tracks the MPPs) is used in the speed regulator input to generate the q-axis current component as shown in Fig. 8. Therefore, a novel SOSMC algorithm is proposed to achieve the speed control of PMSG for each wind speed in order to maximize the extracted power at the turbine output. In this algorithm, the chattering phenomenon can be limited so as to improve the PMSG performance when compared to the classical FOSMC (Fig. 10).

Let us introduce the following sliding surface for the speed Ω.

$$s_{\Omega_t} = \Omega_{tref} - \Omega_t \tag{22}$$

Then we have:

$$\dot{s}_{\Omega_t} = \dot{\Omega}_{tref} - \dot{\Omega}_t = \dot{\Omega}_{tref} - \frac{1}{J}(T_t + T_e - F\Omega_t)$$

If we define the functions G_{Ω_t} as follows:

$$G_{\Omega_t} = \dot{\Omega}_{tref} - \frac{1}{J}(T_t - F\Omega_t)$$

Thus: $\ddot{s}_{\Omega_t} = \dot{G}_{\Omega_t} - \frac{\dot{T}_e}{J}$

The control algorithm proposed which is based on super twisting algorithm (ST) has been introduced by Levant [51].

The second order sliding mode controllers contain two parts:

$$I_{sqref} = I_{sqeq} + I_{sqN} \tag{23}$$

Where: $I_{sqN} = I_1 + I_2$

With: $\begin{cases} \dot{I}_1 = -N_1 sign(s_{\Omega_t}) \\ I_2 = N_2 \sqrt{|s_{\Omega_t}|} sign(s_{\Omega_t}) \end{cases}$

In order to ensure the convergence of the sliding manifolds to zero in finite time, the constants N_1 and N_2 can be chosen as follows [52]:

$$\begin{cases} N_1 > \dfrac{\mu_i}{L_g} \\ N_2 \geq \dfrac{\mu_i(k_i + \mu_i)}{L_g^2(k_i - \mu_i)} \end{cases} \tag{24}$$

2. **Power limit (region III)**

In this region, above the rated wind speed 11.75 m/s as shown in Fig. 11. The control must limit the extracted power in the tolerable beach between $P_l - 1.2P_l$ and the Ω_t of the turbine in the stable operation mode to protect the wind turbine and PMSG, so when the extracted power increases during the nominal value the control circuit shown in Fig. 10, lowered the reference speed, to prevent steady-state high power amounts. A speed controller circuit added to the previous SOSMC-FLC-MPPT design, the sensed stator power as a feedback. When the power exceeds the maximum value, the reference speed must be reduced by the amount, K [53]. The new reference speed $\Omega_{t\,ref\,new}$ is given by:

$$\Omega_{t\,ref\,new} = \Omega_{t\,ref} - \Delta\Omega_t \tag{25}$$

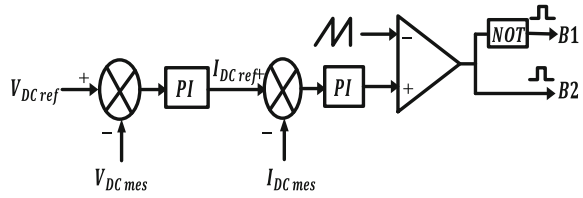## 4.2 Control of the Battery (ESS) Side Converter (BSC)

This converter is controlled in order to maintain the DC bus voltage close to its nominal value (800 v) at different operating conditions (wind speed). Since
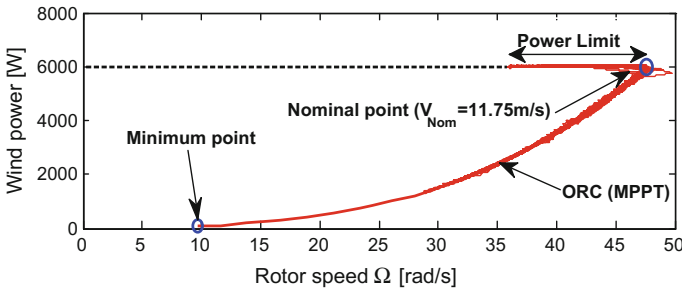
Fig. 11 Real tracking the optimal rotational speed ORC in "region II and III"

Fig. 12 Control block diagram of the Battery ESS

increasing the output power (grid side) rather than the input power to DC-link capacitor (PMSG side) causes a decrease of the ESS voltage and vice versa.

More detailed, Fig. 12, describes the control strategy for the bidirectional DC/DC converter; this controller uses contains two cascaded control loops. The outer control loop compares the measured DC link voltage V_{DC} link to the desired $V_{DC\,ref}$ DC link in order to generate the reference battery current $I_{DC\,ref}$ for the inner control loop. The current $I_{DC\,ref}$ is compared to the measured battery current $I_{DC\,mes}$ in order to generate the gating signals for the IGBT switches. The DC/DC converter charges or discharges the battery according to the duty ratio of the two IGBT switches [54].

The algorithm presented below in Fig. 13 describes excessively different operating modes (charging and discharging of the battery) in nominal and instantaneous variations of the following variables (wind speed (T, N), rated power the turbine (N), the supply and demand side of the network power and the power extracted).
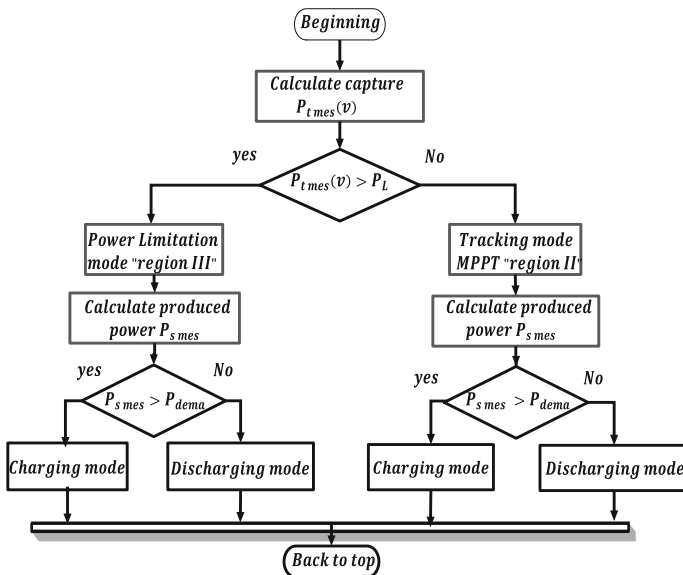
Fig. 13 Flowchart of the charges or discharges cycle in the battery (ESS) side converter

This algorithm is based on the following criteria:

If the power captured by the WT is less than the nominal power of the turbine can select the operating region of the turbine/PMSG by MPPT. In the same case, the power extracted for each wind speed is compared with the power specified by the demand: this means the way of power between the battery and the PMSG (charge or discharge).Otherwise, if the speed exceeds the nominal wind, the operating area of the turbine is moved to the region III, mode 2 (power limitation) and therefore the power produced to be always constant where the load and the system of discharge V_{DC} are imposed by the amount of power required at the electrical grid.

4.3   Control of the Grid Side Converter (GSC)

The main purpose of the GSC is to provide and organized the power required by the user, regardless of the operating conditions. In this part, a new DPC using SOSMC approach and space vector modulation SVM is proposed and realized for the control of the both active and reactive power. Figure 14 shows the schematic diagram of the control of GSC. In the first one, the external loop for controlling the DC link uses a voltage BESS with a bidirectional DC/DC converter is designed.In the task of the second one, internal loop contains an active and reactive power controller based on nonlinear controller SOSMC. The approach of the DPC-SOSMC-SVM strategy directly generates the reference voltage references for the grid side converter unlike the conventional vector method [35].
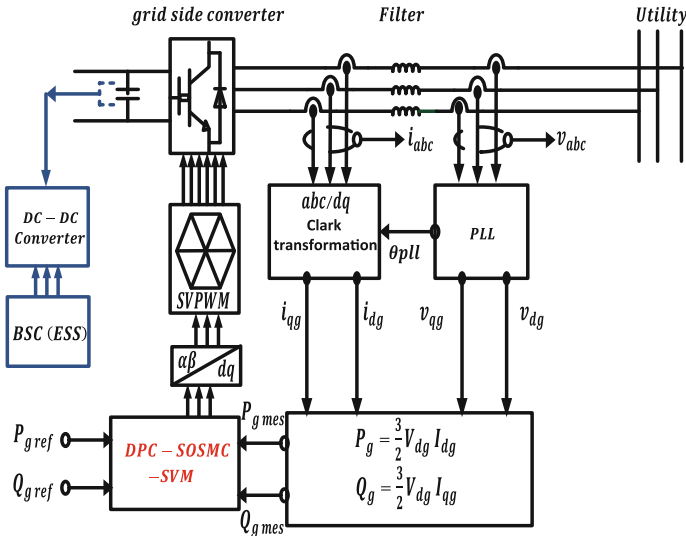

Fig. 14 Control block diagram of grid side converter "DPC-SVM based on SOSMC"

Improved control performance and quality of the power fed to the grid requires advanced and robust control techniques to overcome various constraints. For this reason, a common practice in the treatment of problems of control of the flow of active and reactive power of the grid is to use a conventional linearization approach [55, 56]. However, due to the invisibility of the system uncertainties and external disturbances marring the process control such methods come at the price of poor system performance and low reliability.

To consider these problems, a nonlinear and robust control is required [10, 57–68]. Many methods can be used for this purpose, the SMC control is shown to be particularly suitable for non-linear systems, offering effective structures [11, 21, 22, 30–32].

- **High order sliding mode controller design**

The phenomenon of chattering is the major disadvantage to the practical implementation of a control by sliding mode of order 1. An effective method to deal with this problem is to use a higher order control by sliding mode that generalizes the idea of simple order sliding mode. A command of nth order is the nth derivatives to mitigate the effect chattering keeping the main properties of the original approach as the robustness [69].

The active and reactive grid powers are derived as follows:

$$\begin{cases} P_g = \frac{3}{2} V_{dg} I_{dg} \\ Q_g = \frac{3}{2} V_{dg} I_{qg} \end{cases} \tag{26}$$

The optimal reactive power is set to zero to ensure a unity power factor operation of this system: $Q_{gref} = 0$ whereas the optimal active power P_{gref} can be written depending on the needs of the grid. The block diagram of the SOSMC applied to the grid side converter is illustrated in Fig. 14.

Let us introduce the following sliding surface for the active and reactive powers p_g, Q_g.

$$\begin{cases} s_P = P_{gref} - P_g \\ s_Q = Q_{gref} - Q_g \end{cases} \tag{27}$$

After the first derivation of the both surfaces:
Then we will have

$$\begin{cases} \dot{s}_P = \dot{P}_{gref} - \frac{1.5 V_{dg}}{L_g} \left(-V_{dg} - R_g I_{dg} + L_g w_g I_{qg} \right) - \frac{V_{id}}{L_g} \\ \dot{s}_Q = \dot{Q}_{gref} - \frac{1.5 V_{qg}}{L_g} \left(-V_{qg} - R_g I_{qg} - L_g w_g I_{dg} \right) - \frac{V_{iq}}{L_g} \end{cases} \tag{28}$$

If we define the functions and G_P and G_Q as follows:

$$\begin{cases} G_P = \dot{P}_{gref} - \frac{1.5 V_{dg}}{L_g} \left(-V_{dg} - R_g I_{dg} + L_g w_g I_{qg} \right) \\ G_Q = \dot{Q}_{gref} - \frac{1.5 V_{qg}}{L_g} \left(-V_{qg} - R_g I_{qg} - L_g w_g I_{dg} \right) \end{cases} \tag{29}$$

After the second derivation of the both surfaces:
Thus we have

$$\begin{cases} \ddot{s}_P = \dot{G}_p - \frac{\dot{V}_{id}}{L_g} \\ \ddot{s}_Q = \dot{G}_Q - \frac{V_{iq}}{L_g} \end{cases} \tag{30}$$

The control algorithm proposed which is based on super twisting algorithm (ST) has been introduced by Levant [31]. The second order sliding mode controllers contain two parts:
where

$$\begin{cases} V_P^{ref} = V_p^N + V_p^{eq} \\ V_p^N = w_1 + w_2 \end{cases} \tag{31}$$

with

$$\begin{cases} \dot{w}_1 = -k_1 sign(s_P) \\ w_2 = -M_1 \sqrt{|s_P|} sign(s_P) \end{cases} \tag{32}$$

and

$$\begin{cases} V_Q^{ref} = V_Q^N + V_Q^{eq} \\ V_Q^N = w_1 + w_2 \end{cases} \tag{33}$$

$$\begin{cases} \dot{w}_1 = -k_2 sign(s_Q) \\ w_2 = -M_2 \sqrt{|s_Q|} sign(s_Q) \end{cases} \tag{34}$$

In order to ensure the convergence of the sliding manifolds to zero in finite time, the constants k_i and M_i can be chosen as follows [70].

$$\begin{cases} k_i > \frac{\mu_i}{L_g} \\ M_i \geq \frac{\mu_i(k_i + \mu_i)}{L_g^2(k_i - \mu_i)} \\ |G_i| < \mu_i; i = 1, 2 \end{cases}$$

5 Results and Discussion

The performance of the proposed supervisory control system has been evaluated by numerous simulations (in several areas and in different conditions) using Matlab–Simulink package, under a wind speed profile of (11.75 m/s) mean value as depicted in Fig. 15. The system parameters are given in the Appendix A.
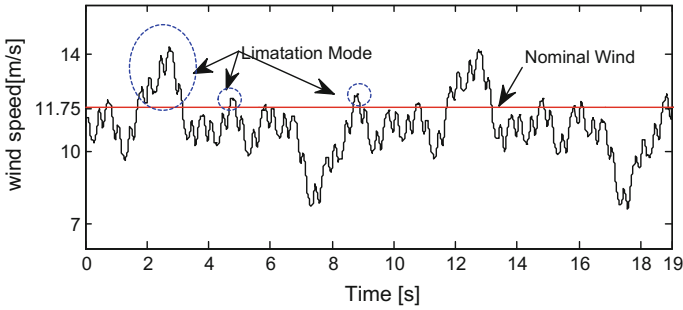
Fig. 15 Wind speed variation in (m/s)

It is noted that in Fig. 15 at nominal wind speed of 11.75 m/s, the WT operates in MPPT Mode (Region II) and the MPPT controller proposed in this paper (FLC-SOSMC-MPPT) ensures the optimum monitoring point of maximum power with high reliability while maintaining the power coefficient to maximum $C_{pmax} = 0.48$ with an optimum value of $\lambda_{opti} = 8.1$, as shown in Figs. 16a, b.

Figure 16c, d, describes the performance of the control law (FLC-SOSMC-MPPT), i.e., the quality of tracking the maximum power point, and one can see the corresponding distribution of the operating point around ORC. From this Figure: a smooth tracking with a high efficiency of the power extracted, with minimal mechanical stress on the turbine shaft.

To protect the wind power generation system (turbine/PMSG) above the rated wind speed (region III), a control mode 2nd was applied (power limitation). Consequently the C_p and λ are reduced. The curve shown in Fig. 16c, demonstrating the reliability and the ability to adapt (switching) of the Control & System in (parts II and III).

The fuzzy logic controller is used to find the optimum speed Ω_{topti} that follows the maximum power point to variable wind speedsin mode 1(tracking mode), also this Ω_{topti} is used as the input to generate a new reference speed $\Omega_{t\,ref\,new}$ in controlmode 2 (power limitation mode).

On the other hand, a SOSMC algorithm is then applied to control the speed of a PMSG, the robustness of which is investigated and finally the performance of the SOSMC is compared with that obtained by a FOSMC as illustrated in Fig. 17a. In both regions, two controllers are able to track the desired slip trajectory precisely which is an inherent advantage of the sliding mode controller. However, the result using conventional FOSMC shows some chattering in all the response as illustrated in Fig. 17a, this phenomenon is highly undesirable as it may lead to vibration on the mechanical part (high-frequency mechanical efforts on the turbine shaft). The SOSMC, on the other hand, get rid of the chattering phenomenon, giving a smooth tracking trajectory and lower slip error and lower control effort as it can be seen in Fig. 17b, where the value for the speed error is limited by a maximum value [0.1, −0.1] rad/s (negligible error).
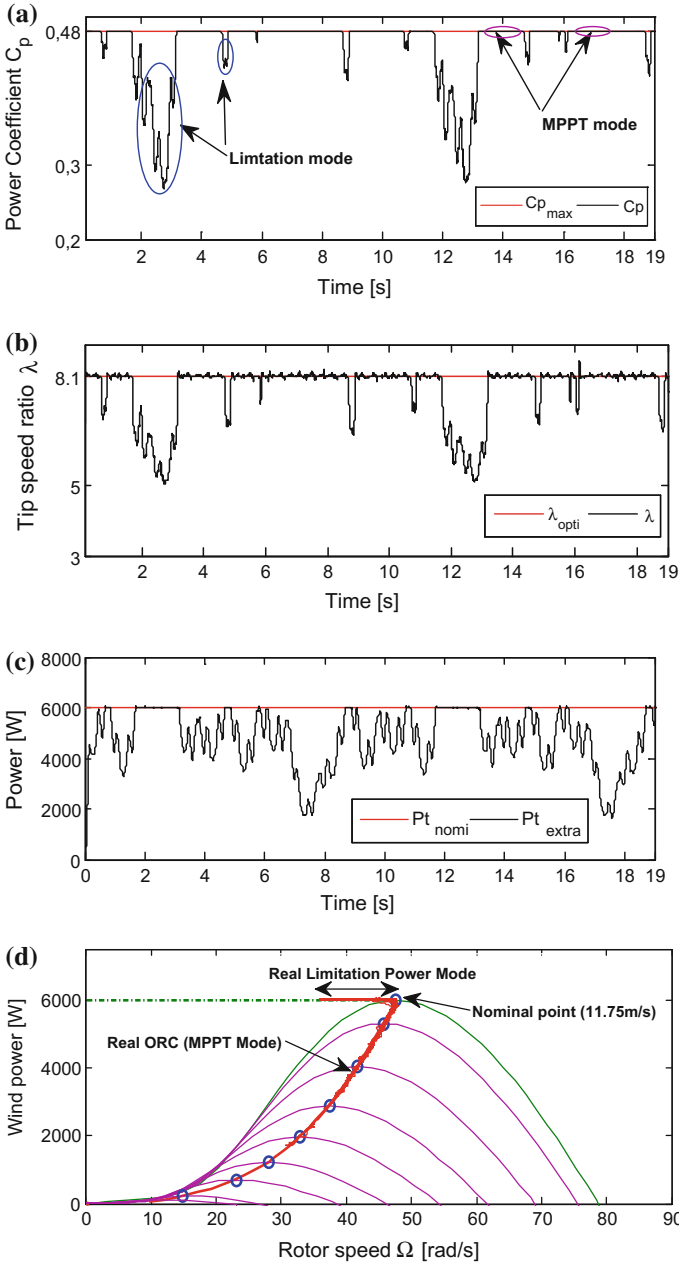
Fig. 16 MPPT FLC-SOSMC, **a** Power coefficient C_p, **b** The tip speed ratio λ, **c** The power generation in both region (II, III) and **d** The real power characteristic of the WT used in this study (II and III)
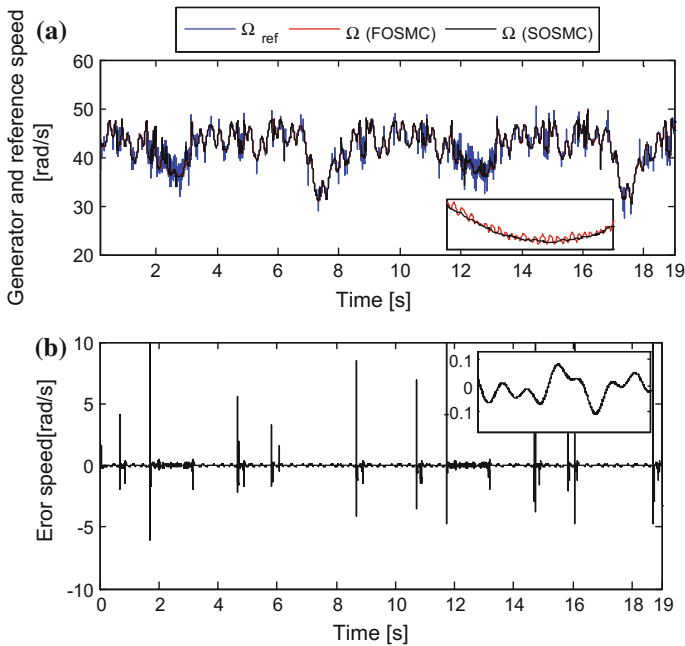
Fig. 17 **a** Generator speed used (FOSMC/SOSMC) and **b** Error speed

Under instantaneous variation for the (generated power, power demand), the battery is used to stabilize the voltage at the PMSG DC bus, the second main task of the control system is to maintain the DC Link voltage close to its nominal value 800 V, as it can be seen in Fig. 18a, by designing a battery DC/DC power converter for this purpose. The active power response, measured at different points of the hybrid system (in region II and III, is shown in Fig. 18b, c.

The requested power (demand power 'reference') is initially set to 3000 W in the first (5 s). A t = 5 s, the demand is increased to a value up to 4000 W t = 10 s and after she continues to increase to 7000 W during the period of [10–14 s], finally an decreased of 5000 W has been produced in the rest of the simulation time [14–19 s] as shown in Fig. 18b, c. In all cases we take into consideration the operating area of WT (2 or 3).

1. From [0 s to 5 s] as shown in Fig. 18b, c. The active power demanded by the grid is $P_{deman} = 3000W$. During this period, the reference power is lower than the available wind power [$P_{deman} < P_{extr}$]. At that moment, a battery recharging cycle begins and lasts until the SOC achieved 50.048% or higher. During the recharging time, the battery is charged by the power surplus provided by the PMSG. The advantage of storing excess wind power has become an important option in the field of WTs.

(a)

(b)

(c)

(d)
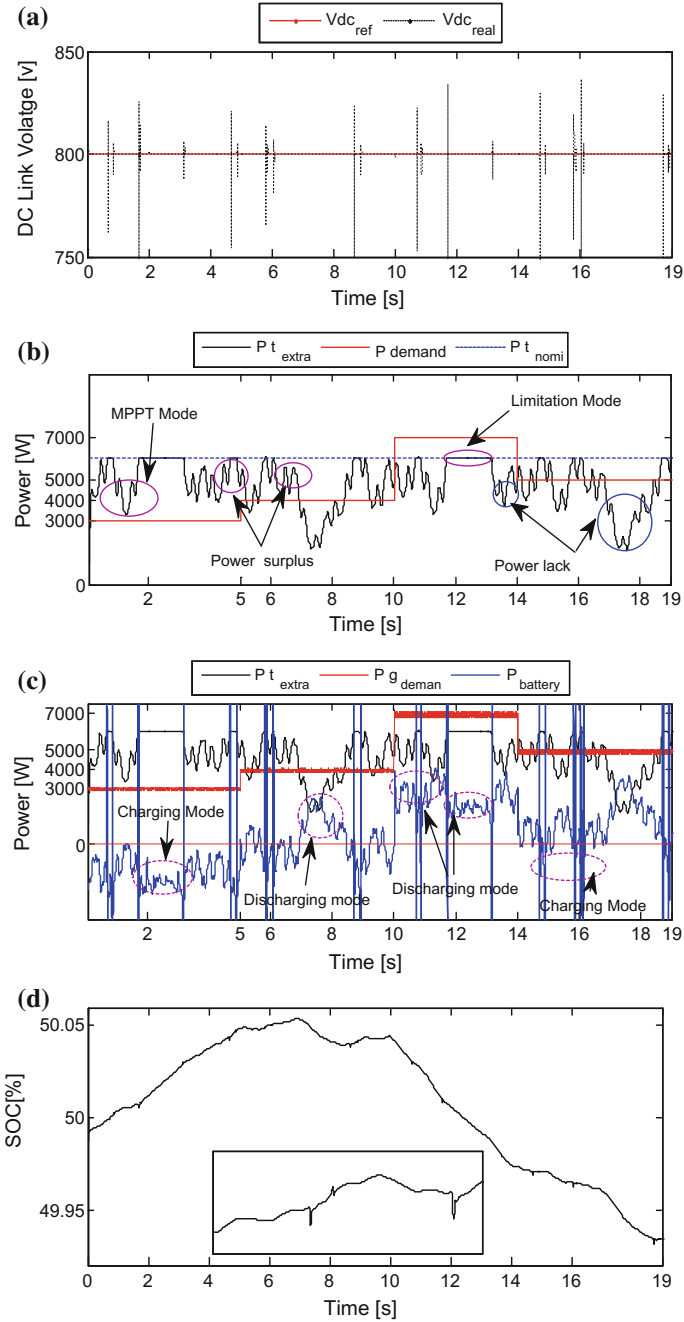
Fig. 18 ESS control **a** DC link voltage, **b** 'extrcted, nominal, demand' active power, **c** 'grid, battery, extracted' active power and **d** SOC of Battery

2. For instance we find, from [5 s s to 10 s], the active power demanded by the grid is $P_{deman} = 4000W$(a predetermined value) which is "lower or higher" the available wind power as presented in Fig. 18b, c. For this reason: First, when the active power demanded by the grid is higher [$P_{deman} > P_{extr}$], than the available wind power(extracted power), the battery supplements (discharging mode) the output of PMSG in order to provide the demanded power until it reaches its lowest recommended SOC of 50.03%. Then, when the power demanded by the grid is lower [$P_{deman} < P_{extr}$], below the available wind power, this power surplus provided by the PMSG is also stored in the battery (charging mode), enabling SOC to increase (50.044%) as observed in Fig. 18d.

3. During the period [10–14 s] where the demand for power is 7000 W maximum, the latter is greater than the power extracted by the turbine [$P_{deman} > P_{extr}$] as observed in Fig. 18b, c. In this case, the ESS provides electrical power (discharging mode) to compensate for lack of the power supplied to the power grid (the gap between demand and production). During this period, a battery discharge cycle begins and lasts until 14 s, and a remarkable decrease in SOC continues up to 49.97% as illustrated in Fig. 18d. This hybrid system is able to work in unpredictable conditions and overcoming various constraints. According to Fig. 18b, c.

4. The same phenomena of the first interval [5–10 s] is similar to the during the time interval [14–19 s]. During the period [14–19 s] where the demand for power is 5000 W, the latter or lower is greater than the power extracted by the turbine $P_{deman} > < P_{extr}$ as observed in Fig. 18b, c. In this case, the ESS (provides/absorbed) electrical power (discharging/charging) to compensate or store for (lack/surplus) of the power (supplied to the grid/provided by the PMSG).

This hybrid system is able to work in unpredictable conditions (region II or III) and overcoming various constraints. According to Fig. 18d. In the previous four steps, SOS rapidly varied to achieve every moment the cycles of charge/discharge of the battery.

In the last one: active and reactive power control has been achieved by direct power control DPC-SVM.

To assess the merit of our choice SOSMC, a comparison was made between four types of controllers (PI conventional, fractional PI, FOSMC and SOSMC), these controllers are compared with a separately [(PI/PI$_{fractional}$) (FOSMC/SOSMC) and (PI$_{fractional}$/SOSMC)] for objective to clarify their efficacy compared to our selection. Other shares, these results are supported by a harmonic analysis of each regulator as shown in Table 2.

**Table 2** A comparison of the four Controller types

Controller types	PI (conventional)	PI (fractional)	FOSMC	SOSMC
Current THD	3.96%	0.93%	3.86%	**0.59%**

Figures 19 and 20 display the (active and reactive powers) on the grid side, controlled via the proposed DPC-SVM and used four different types of regulators.

From Figs. 19a and 20a, both types of controllers (SOSMC) and (FOSMC) are able to track the desired slip trajectory precisely but, under the super twister control algorithm, the (direct, quadrature currents and active, reactive powers grid) track their reference values with chattering-free smooth profiles. By comparison, the result of the conventional FOSMC shows some chattering in all the responses. This phenomenon is highly undesirable as it may produce current distortion. The reactive power is set at zero for unity power factor is shown in Fig. 20a.
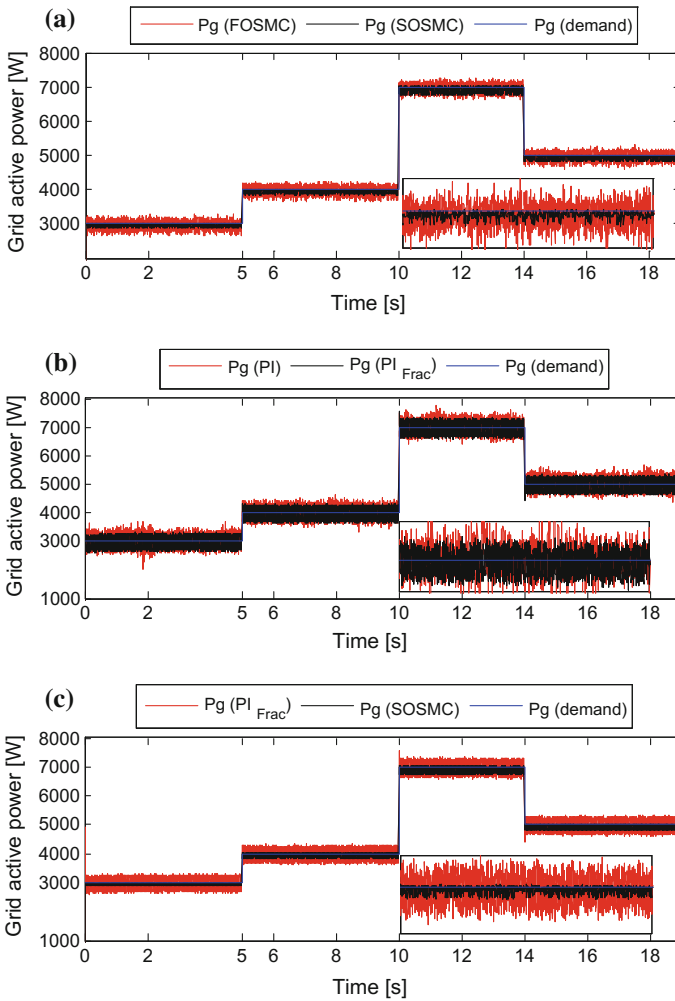
Fig. 19 Grid active power used DPC-SVM, **a** "FOSMC/SOSMC", **b** "PI/PI frac'' and **c** "SOSMC/PI frac"
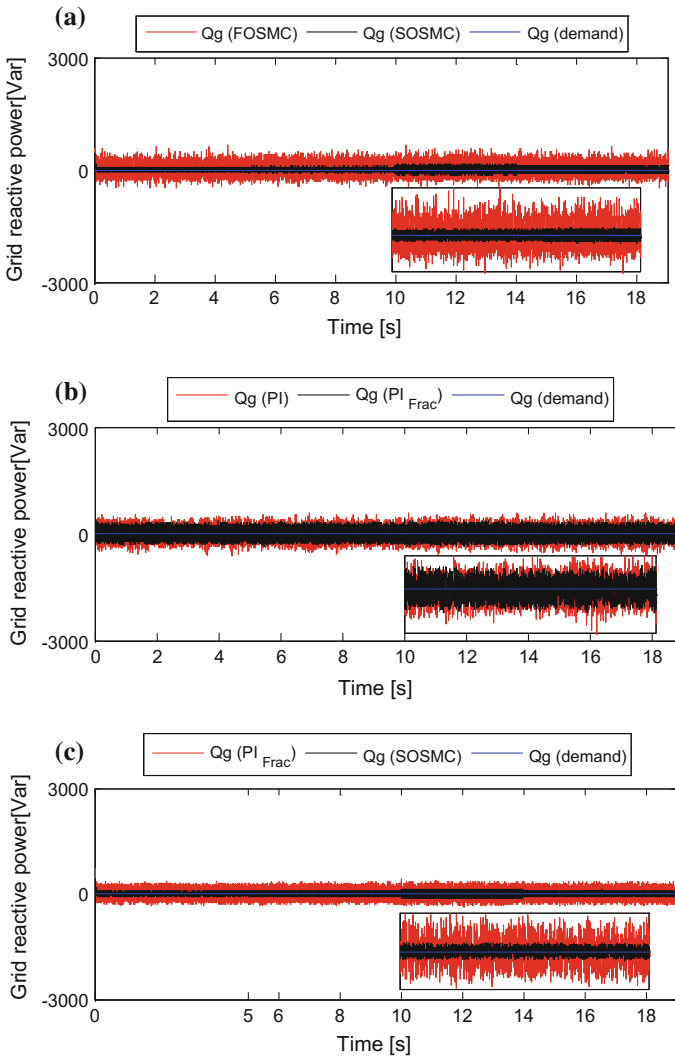
Fig. 20 Grid active power used DPC-SVM, **a** "FOSMC/SOSMC", **b** "PI/PI frac'' and **c** "SOSMC/PI frac"

While comparatively, the Figs. 19b and 20b describes these quantities (grid active and reactive power) under the conventional PI and PI fractional. From these figures we have observed that the two controllers are able to track the desired reference precisely with a clear priority to the PI fractional controller.

Figures 19c and 20c assembly the two best resulting regulators (SOSMC, PI$_{fractional}$) in "Figs. 19a, b and 20a, b", this comparison are given a general way the reason and contentment of our choice of the (SOMSC) controller. After these
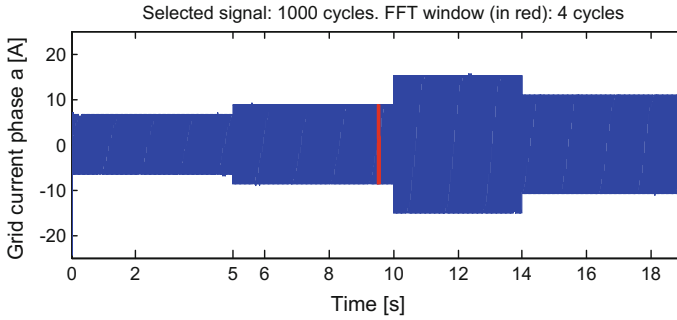
Fig. 21 Grid current phase "A"
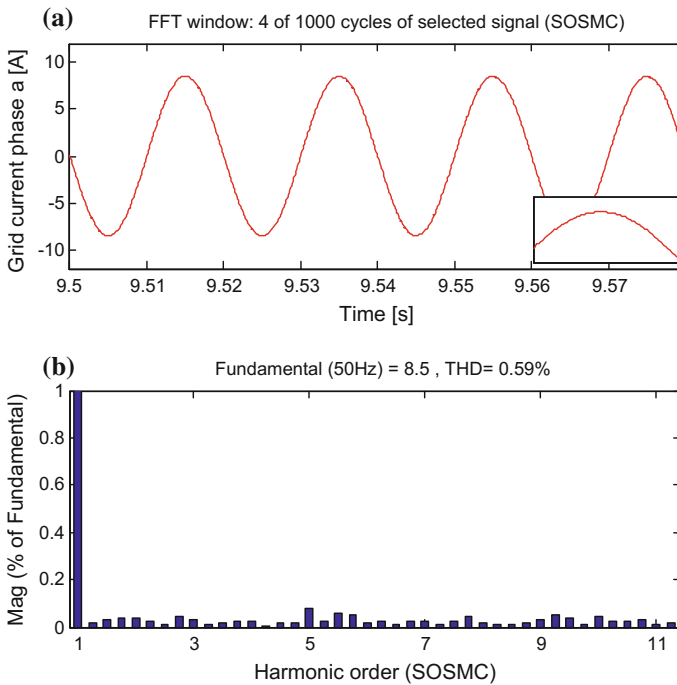
Fig. 22 a Grid current for SOSMC, **b** THD for SOSMC

Figures we have observed a high efficiency and smooth to track the desired slip trajectory precisely unlike the "PI$_{fractional}$".

The results obtained in this section show a good performance to follow the desired path (active and reactive power) compared to conventional regulators such as (FOSMC, PI and PI$_{fractional}$).
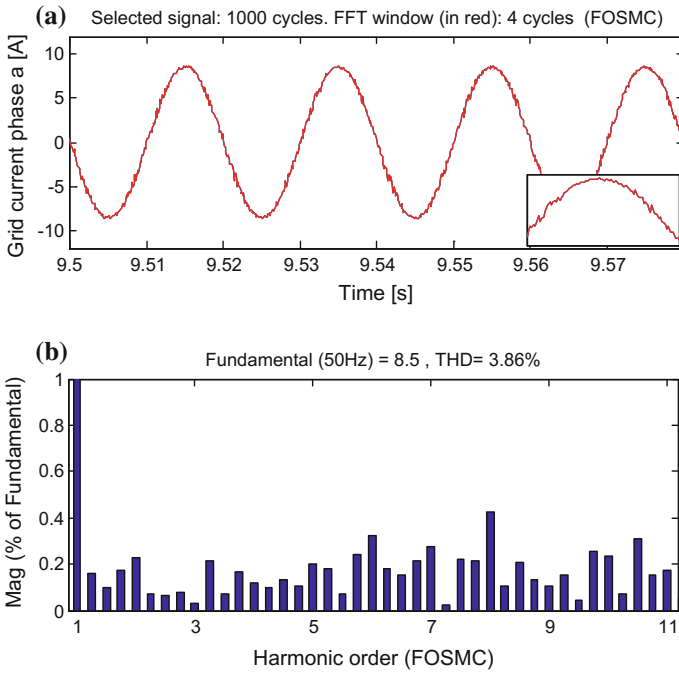
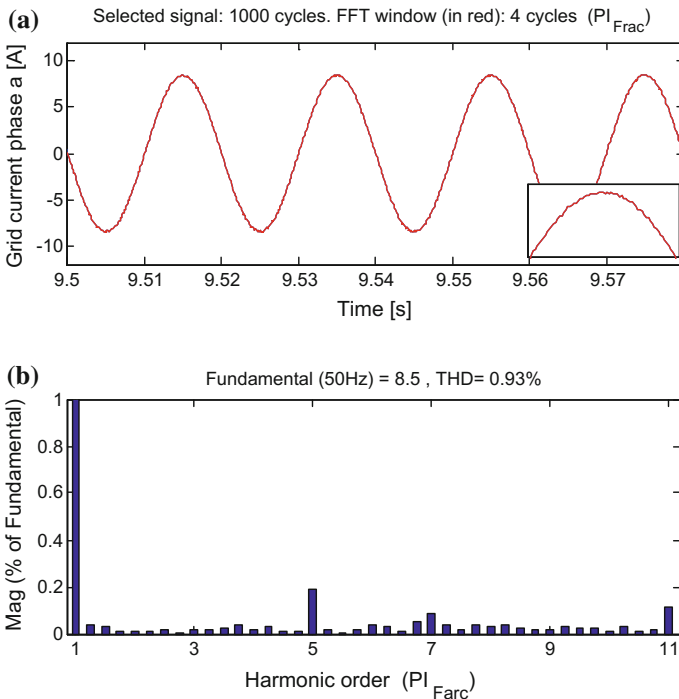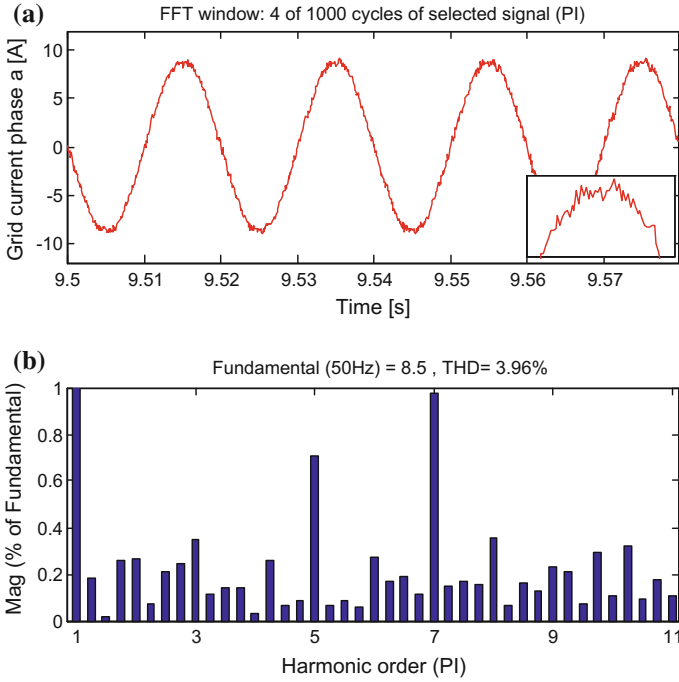**Fig. 23** **a** Grid current for FOSMC, **b** THD for FOSMC

Fig. 24 **a** Grid current for PI frac, **b** THD for PI frac

Fig. 25 **a** Grid current for PI conventional, **b** THD for PI conventional

Figure 21 illustrates a sample waveform of the grid current for phase A. To see the efficiency of the proposed control strategy (SOMSC), a Harmonic frequency spectrum and total harmonic distortion (THD) of the grid current controlled by (SOSMC, FOSMC, PI$_{frac}$ and PI) controllers are shown in Figs. 22, 23, 24, and 25a, b. The THD shown in Figs. 23(b) and Fig. 25b are bigger and reaches 3.86% and 3.96% respectively.

That means, some unwanted distortion in the current waveform as shown in Figs. 23a and 25a, it means a poor quality of the power delivered to the power grid when we use (PI$_{conventional}$ and FOSMC). Compared with (SOSMC/PI$_{fractional}$) Where is reduced THD (0.59% and 0.93%) respectively as summarized in Table 2. In the proposed control system (SOMSC), we noticed that the distortion of the electrical current no longer appears Fig. 22a. This efficiency is due to the elimination by filtering odd harmonics Fig. 22b.

In Table 2, A comparison of the four strategies of controller types is summarized. The current THD shows that an important improvement in terms of odd harmonic mitigation (3–11). It can be concluded that the proposed method (SOMSC) can filter more than 80 and 40% of single harmonics compared to classical methods (FOSMC, PI$_{conventional}$) and (PI$_{fractional}$).

6   Conclusion and Future Work

Wind speed is often considered as one of the most difficult parameters to estimate because of its intermittent, which can deviate quickly. Although much effort has been dedicated to make WTs in wide operating range (to include more than one region at the same time).

In this chapter, a novel supervisory control scheme has been proposed to optimize the power management of a hybrid renewable energy system in the both regions (II and III) and to evaluate the coordinate operation of a grid connected of PMSG wind turbine and BESS.

In comparison with the existing works, our proposed architecture of control systems (supervisory control) provide to the WTs a freedom to work in a wide range with high protection in rated wind speed. The effectiveness of the control architecture has been checked by simulation study and compared to conventional control techniques, the proposed configuration considered was tested under varied operating conditions.

The significance of this work is indicated below:

a. *System Design*

- The WT proposed in this study is (Horizontal-axis/variable speed wind turbine/three-bladed).
- Due to its simple structure with characteristic self-excitation that can work with. The PMSG is nowadays a popular choice for variable speed WTs.
- Due to the inherently sporadic nature of the wind which can deviate quickly. The utilization of the BESS in WT increases the safe operation of the power grid, balance the supply and demand sides.
- The three converters are controlled precisely to mitigate grid power disturbances and ensure the maximum power extraction for each wind speed.

b. *control system Design*

- The generator side controller used to track and limited the maximum power generated from WT by controlling the rotational speed of the PMSG in the (region II and III) for this reason a FLC-SOSMC were designed to extract the maximum aerodynamic power up to the rated power (tracking mode), regardless of the turbine power-speed slope. If the wind power exceeds the rated value, the system switches to power regulation mode, via the power limitation circuit (limitation power mode).
- The battery DC/DC converter is controlled to maintain the DC bus voltage at its rated value. The ESS provides or stores the power mismatching between the actual wind power and grid demand. As a result, the hybrid system is

able to provide constant power to the grid as the incoming wind varies and increases the power transferred to the grid when required.

- In the grid side converter, the described DPC-SVM based on high order SMC has been designed to control the active and reactive powers exchanged between the PMSG and the grid. On the other hand, the grid power quantities provided by the SOSMC strategy shows smooth waveforms with good tracking indices and small THD compared with (FOSMC, $PI_{conventional}$ and $PI_{fractional}$).

c. *Results judged (obtained contribution)*

- It can be judged that the proposed structure (VSWT, PMSG, BESS) along with the integrating of the supervisory control strategy based on robust nonlinear techniques (FLC, SOSMC) turns the classical system into an enhanced stable, reliable and effective hybrid system with uniform protection, ensuring the power quality and management in the system under various operating conditions (region II and III).

d. *Future work*

- In future research, the authors wish to explore a methodology to store excess wind power when the BESS is in a state of saturation, there is more wind power and a decrease in demand.
- In addition, the present work focused on the implementation of efficient and robust control system for power management (limitation, tracking and delivered) by the wind hybrid system. To evaluates this work, the experimental results are necessary (test bench).
- We also plan to implement this method on several proposed wind turbines (small wind farm with high power), with optimization in untreated Points by others as: intelligent control for limiting the power in rated wind speeds or above par and controlling the AC/DC/AC.

Appendix A

Tables 3, 4 and 5.

Table 3 Nomenclatures and Abbreviations

Nomenclature	
$V_{sd}, V_{sq}, I_{sd}, I_{sq}$	The direct and quadrature components of the PMSG voltages and currents respectively
R_s, L_d, L_q	The resistance, the direct and the quadrature inductance of the PMSG respectively
ψ_m	The magneticflux
T_e	The electromagnetic torque
ω_e	The electrical rotational speed of PMSG
n_p	The number of pole pairs
$V_{dg}, V_{qg}, I_{dg}, I_{qg}$	The direct and quadrature components of the grid voltages and currents respectively
V_{di}, V_{qi}	The inverter voltages components
R_g, L_{dg}, L_{qg}	The resistance, the direct and quadrature grid inductance respectively
V_{bat}, E_0	The battery rated voltage and the internal EMF respectively
$E_{batdisch}, E_{batcharg}$	The discharge and charge voltage respectively
R_i, Q	The internal resistance and the battery capacity respectively
i_t, i^*	The actual battery charge and the filtered current respectively
BESS	The battery energy storage system
WTG	The wind turbine generator
MPP	The maximum power point
FLC	The fuzzylogiccontroller
SOSMC	The second order sliding mode control
FOSMC	The first order sliding controller
WECS	The wind energy conversion system
PMSG	The permanent magnetsynchronousgenerators
MPPT	The Maximum Power Point Tracking
ESS	The energystorage system
TSR	The tip speed ratio
HCS	The hill-climbsearching
MSC	The machine sideconverter
GSC	The gridsideconverter
BSC	The batterysideconverter
WT	The wind turbine

Table 4 PMSG parameters

Nominal power	$P = 6$ kw
Stator resistance	$R_s = 0.4\ \Omega$
Direct stator inductance	$L_d = 8.4$ mH
Stator inductance quadrature	$L_q = 8.4$ mH
Field flux	$\psi_{fl} = 0.4$ wb
Number of pole pairs	$n_p = 12$
Inertia	$J_t = 0.089$ kg.m^2
Friction	$f = 0.0016$ N.m

Table 5 Wind turbine parameters

Radius of the turbine	$R_t = 3.2$ m
Volume density of the air	$\rho = 1.225$ kg.m^3
The pitch angle	$\beta = 0°$
specific optimal speed	$\lambda_{opti} = 8.1$
Coefficient of maximum power	$C_{pmax} = 0.48$

References

1. Nikolova, S., Causevski, A., & Al-Salaymeh, A. (2013). Optimal operation of conventional power plants in power system with integrated renewable energy sources. *Energy Conversion and Management, 65*(2013), 697–703.
2. Zou, Y., Elbuluk, M. E., & Sozer, Y. (2013). Simulation comparisons and implementation of induction generator wind power systems. *IEEE Transactions on Industry Applications, 49*(3), 1119–1128.
3. Carranza, O., Figueres, E., Garcerá, G., & Gonzalez-Medina, R. (2013). Analysis of the control structure of wind energy generation systems based on a permanent magnet synchronous generator. *Applied Energy, 103*(2013), 522–538.
4. Aissaoui, A. G., Tahour, A., Essounbouli, N., Nollet, F., Abid, M., & Chergui, M. I. (2013). A Fuzzy-PI control to extract an optimal power from wind turbine. *Energy Conversion and Management, 65*(2013), 688–696.
5. Abdullah, M. A., Yatim, A. H. M., Tan, C. W., et al. (2012). A review of maximum power point tracking algorithms for wind energy systems. *Renewable and Sustainable Energy Reviews, 16*(5), 3220–3227.
6. Jaramillo-Lopez, F., Kenne, G., & Lamnabhi-Lagarrigue, F. (2016). A novel online training neural network-based algorithm for wind speed estimation and adaptive control of PMSG wind turbine system for maximum power extraction. *Renewable Energy, 86*(2016), 38–48.
7. Syed, I. M., Venkatesh, B., Wu, B., & Nassif, A. B. (2012). Two-layer control scheme for a supercapacitor energy storage system coupled to a Doubly fed induction generator. *Electric Power Systems Research, 86*(2012), 76–83.
8. Domínguez-García, J. L., Gomis-Bellmunt, O., Bianchi, F. D., & Sumper, A. (2012). Power oscillation damping supported by wind power: a review. *Renewable and Sustainable Energy Reviews, 16*(7), 4994–5006.
9. Zhao, H., Wu, Q., Hu, S., Xu, H., & Rasmussen, C. N. (2015). Review of energy storage system for wind power integration support. *Applied Energy, 137*(2015), 545–553.
10. Azar, A. T., & Zhu, Q. (2015). *Advances and Applications In Sliding Mode Control Systems. Studies in computational intelligence* (vol. 576). Germany: Springer. ISBN: 978-3-319-11172-8.
11. Abdeddaim, S., & Betka, A. (2013). Optimal tracking and robust power control of the DFIG wind turbine. *International Journal of Electrical Power & Energy Systems, 49*(2013), 234–242.
12. Gao, R., & Gao, Z. (2016). Pitch control for wind turbine systems using optimization, estimation and compensation. *Renewable Energy, 91*(2016), 501–515.
13. Kumar, A., & Verma, V. (2016). Photovoltaic-grid hybrid power fed pump drive operation for curbing the intermittency in PV power generation with grid side limited power conditioning. *International Journal of Electrical Power & Energy Systems, 82*(2016), 409–419.
14. Yin, X. X., Lin, Y. G., Li, W., Liu, H. W., & Gu, Y. J. (2015). Adaptive sliding mode back-stepping pitch angle control of a variable-displacement pump controlled pitch system for wind turbines. *ISA Transactions, 58*(2015), 629–634.

15. Saravanakumar, R., & Jena, D. (2015). Validation of an integral sliding mode control for optimal control of a three blade variable speed variable pitch wind turbine. *International Journal of Electrical Power & Energy Systems, 69*(2015), 421–429.

16. Kim, H., Son, J., & Lee, J. (2011). A high-speed sliding-mode observer for the sensorless speed control of a PMSM. *IEEE Transactions on Industrial Electronics, 58*(9), 4069–4077.

17. Ramesh, T., Panda, A. K., & Kumar, S. S. (2015). Type-2 fuzzy logic control based MRAS speed estimator for speed sensorless direct torque and flux control of an induction motor drive. *ISA Transactions, 57*(2915), 262–275.

18. Thirusakthimurugan, P., & Dananjayan, P. (2007). A novel robust speed controller scheme for PMBLDC motor. *ISA Transactions, 46*(4), 471–477.

19. Pichan, M., Rastegar, H., & Monfared, M. (2013). Two fuzzy-based direct power control strategies for doubly-fed induction generators in wind energy conversion systems. *Energy, 51* (2013), 154–162.

20. Uhlen, K., Foss, B. A., & Gjøsæter, O. B. (1994). Robust control and analysis of a wind-diesel hybrid power plant. *IEEE Transactions on Energy Conversion, 9*(4), 701–708.

21. Evangelista, C., Valenciaga, F., & Puleston, P. (2013). Active and reactive power control for wind turbine based on a MIMO 2-sliding mode algorithm with variable gains. *IEEE Transactions on Energy Conversion, 28*(3), 682–689.

22. Billela, M., Dib, D., & Azar, A. T. (2016). A Second order sliding mode and fuzzy logic control to Optimal Energy Management in PMSG Wind Turbine with Battery Storage. In *Neural Computing and Applications*. Springer. doi:10.1007/s00521-015-2161-z.

23. Assareh, E., & Biglari, M. (2015). A novel approach to capture the maximum power from variable speed wind turbines using PI controller, RBF neural network and GSA evolutionary algorithm. *Renewable and Sustainable Energy Reviews, 51*(2015), 1023–1037.

24. Witczak, P., Patan, K., Witczak, M., Puig, V., & Korbicz, J. (2015). A neural network-based robust unknown input observer design: Application to wind turbine. *IFAC-PapersOnLine, 48* (21), 263–270.

25. Ata, R. (2015). Artificial neural networks applications in wind energy systems: a review. *Renewable and Sustainable Energy Reviews, 49*(2015), 534–562.

26. Suganthi, L., Iniyan, S., & Samuel, A. A. (2015). Applications of fuzzy logic in renewable energy systems–A review. *Renewable and Sustainable Energy Reviews, 48*(2015), 585–607.

27. Banerjee, A., Mukherjee, V., & Ghoshal, S. P. (2014). Intelligent fuzzy-based reactive power compensation of an isolated hybrid power system. *International Journal of Electrical Power & Energy Systems, 57*(2014), 164–177.

28. Castillo, O., & Melin, P. (2014). A review on interval type-2 fuzzy logic applications in intelligent control. *Information Sciences, 279*(2014), 615–631.

29. Mérida, J., Aguilar, L. T., & Dávila, J. (2014). Analysis and synthesis of sliding mode control for large scale variable speed wind turbine for power optimization. *Renewable Energy, 71* (2014), 715–728.

30. Hong, C.-M., Huang, C.-H., & Cheng, F.-S. (2014). Sliding Mode Control for Variable-speed Wind Turbine Generation Systems Using Artificial Neural Network. *Energy Procedia, 61* (2014), 1626–1629.

31. Benbouzid, M., Beltran, B., Amirat, Y., Yao, G., Han, J., & Mangel, H. (2014). Second-order sliding mode control for DFIG-based wind turbines fault ride-through capability enhancement. *ISA Transactions, 53*(3), 827–833.

32. Liu, J., Lin, W., Alsaadi, F., & Hayat, T. (2015). Nonlinear observer design for PEM fuel cell power systems via second order sliding mode technique. *Neurocomputing, 168*(2015), 145–151.

33. Evangelista, C. A., Valenciaga, F., & Puleston, P. (2012). Multivariable 2-sliding mode control for a wind energy system based on a double fed induction generator. *International Journal of Hydrogen Energy, 37*(13), 10070–10075.

34. Eltamaly, A. M., & Farh, H. M. (2013). Maximum power extraction from wind energy system based on fuzzy logic control. *Electric Power Systems Research, 97*(2013), 144–150.
35. Meghni, B., Saadoun, A., Dib, D., & Amirat, Y. (2015). Effective MPPT technique and robust power control of the PMSG wind turbine. *IEEJ Transactions on Electrical and Electronic Engineering, 10*(6), 619–627.
36. Sarrias, R., Fernández, L. M., García, C. A., & Jurado, F. (2012). Coordinate operation of power sources in a doubly-fed induction generator wind turbine/battery hybrid power system. *Journal of Power Sources, 205*(2012), 354–366.
37. Sarrias-Mena, R., Fernández-Ramírez, L. M., García-Vázquez, C. A., & Jurado, F. (2014). Improving grid integration of wind turbines by using secondary batteries. *Renewable and Sustainable Energy Reviews, 34*(2014), 194–207.
38. Sharma, P., Sulkowski, W., & Hoff, B. (2013). Dynamic stability study of an isolated wind-diesel hybrid power system with wind power generation using IG, PMIG and PMSG: A comparison. *International Journal of Electrical Power & Energy Systems, 53*(2013), 857–866.
39. Liu, J., Meng, H., Hu, Y., Lin, Z., & Wang, W. (2015). A novel MPPT method for enhancing energy conversion efficiency taking power smoothing into account. *Energy Conversion and Management, 10*(2015), 738–748.
40. Nasiri, M., Milimonfared, J., & Fathi, S. H. (2014). Modeling, analysis and comparison of TSR and OTC methods for MPPT and power smoothing in permanent magnet synchronous generator-based wind turbines. *Energy Conversion and Management, 86*(2014), 892–900.
41. Daili, Y., Gaubert, J.-P., & Rahmani, L. (2015). Implementation of a new maximum power point tracking control strategy for small wind energy conversion systems without mechanical sensors. *Energy Conversion and Management, 97*(2015), 298–306.
42. Kortabarria, I., Andreu, J., de Alegría, I. M., Jiménez, J., Gárate, J. I., & Robles, E. (2014). A novel adaptative maximum power point tracking algorithm for small wind turbines. *Renewable Energy, 63*(2014), 785–796.
43. Ghedamsi, K., & Aouzellag, D. (2010). Improvement of the performances for wind energy conversions systems. *International Journal of Electrical Power & Energy Systems, 32*(9), 936–945.
44. Poitiers, F., Bouaouiche, T., & Machmoum, M. (2009). Advanced control of a doubly-fed induction generator for wind energy conversion. *Electric Power Systems Research, 79*(7), 1085–1096.
45. Hong, C.-M., Chen, C.-H., & Tu, C.-S. (2013). Maximum power point tracking-based control algorithm for PMSG wind generation system without mechanical sensors. *Energy Conversion and Management, 69*(2013), 58–67.
46. Zou, Y., Elbuluk, M., & Sozer, Y. (2013). Stability analysis of maximum power point tracking (MPPT) method in wind power systems. *IEEE Transactions on Industry Applications, 49*(3), 1129–1136.
47. Narayana, M., Putrus, G. A., Jovanovic, M., Leung, P. S., & McDonald, S. (2012). Generic maximum power point tracking controller for small-scale wind turbines. *Renewable Energy, 44*(2012), 72–79.
48. Yin, M., Li, G., Zhou, M., & Zhao, C. (2007). Modeling of the wind turbine with a permanent magnet synchronous generator for integration. In *Power Engineering Society General Meeting, IEEE 2007*, June 24-28, 2007, Tampa, FL, (pp. 1–6). doi:10.1109/PES.2007.385982.
49. SimPowerSystems, T. M. (2010). Reference, Hydro-Qu{é}bec and the MathWorks. Inc., Natick, MA.
50. Jain, B., Jain, S., & Nema, R. K. (2015). Control strategies of grid interfaced wind energy conversion system: An overview. *Renewable and Sustainable Energy Reviews, 47*(2015), 983–996.

51. Benelghali, S., El Hachemi Benbouzid, M., Charpentier, J. F., Ahmed-Ali, T., & Munteanu, I. (2011). Experimental validation of a marine current turbine simulator: Application to a permanent magnet synchronous generator-based system second-order sliding mode control. *IEEE Transactions on Industrial Electronics, 58*(1), 118–126.

52. Rafiq, M., Rehman, S., Rehman, F., Butt, Q. R., & Awan, I. (2012). A second order sliding mode control design of a switched reluctance motor using super twisting algorithm. *Simulation Modelling Practice and Theory, 25*(2012), 106–117.

53. Soler, J., Daroqui, E., Gimeno, F.J., Seguí-Chilet, S., & Orts, S. (2005). Analog low cost maximum power point tracking PWM circuit for DC loads. In *Proceedings of the Fifth IASTED International Conference on Power and Energy Sysemst, Benalmadena,* Spain, June 15–17, 2005.

54. Gkavanoudis, S. I., & Demoulias, C. S. (2014). A combined fault ride-through and power smoothing control method for full-converter wind turbines employing Supercapacitor Energy Storage System. *Electric Power Systems Research, 106*(2014), 62–72.

55. Pena, R., Cardenas, R., Proboste, J., Asher, G., & Clare, J. (2008). Sensorless control of doubly-fed induction generators using a rotor-current-based MRAS observer. *IEEE Transactions on Industrial Electronics, 55*(1), 330–339.

56. Tapia, G., Tapia, A., & Ostolaza, J. X. (2007). Proportional–integral regulator-based approach to wind farm reactive power management for secondary voltage control. *IEEE Transactions on Energy Conversion, 22*(2), 488–498.

57. Azar, A. T. (2012). Overview of type-2 fuzzy logic systems. *International Journal of Fuzzy System Applications, 2*(4), 1–28.

58. Azar, A. T. (2010). *Fuzzy systems*. Vienna: IN-TECH. ISBN 978-953-7619-92-3.

59. Azar, A.T., & Vaidyanathan, S. (2015). Handbook of research on advanced intelligent control engineering and automation. In *Advances in Computational Intelligence and Robotics (ACIR) Book Series*, IGI Global, USA.

60. Azar, A. T., & Vaidyanathan, S. (2015). *Computational intelligence applications in modeling and control*. Studies in computational intelligence (vol. 575). Germany: Springer. ISBN 978-3-31911016-5.

61. Azar, A. T., & Vaidyanathan, S. (2015). *Chaos modeling and control systems design, studies in computational intelligence* (Vol. 581). Germany: Springer. ISBN 978-3-319-13131-3.

62. Zhu, Q., & Azar, A. T. (2015). Complex system modelling and control through intelligent soft computations. *Studies in fuzziness and soft computing* (vol. 319). Germany: Springer. ISBN: 978-3-31912882-5 123.

63. Azar, A.T., & Serrano, F.E. (2015). Design and modeling of anti wind up PID controllers. In Q. Zhu & A. T. Azar (Eds.), *Complex system modelling and control through intelligent soft computations, Studies in Fuzziness and Soft Computing* (vol. 319, pp. 1–44). Germany: Springer, Germany. doi:10.1007/978-3-319-12883-2_1.

64. Azar, A. T., & Serrano, F. E. (2015). Adaptive sliding mode control of the furuta pendulum. In A. T. Azar & Q. Zhu, (Eds.) *Advances and Applications in Sliding Mode Control systems, Studies in Computational Intelligence*, (vol. 576, pp. 1–42). Berlin/Heidelberg: Springer GmbH. doi:10.1007/978-3-319-11173-5_1.

65. Azar, A. T., & Serrano, F. E. (2015). Deadbeat control for multivariable systems with time varying delays. In A. T. Azar & S. Vaidyanathan (Eds.), *Chaos modeling and control systems design, studies in computational intelligence* (vol 581, pp 97–132). Berlin: Springer GmbH. doi:10.1007/978-3-319-13132-0_6.

66. Mekki, H., Boukhetala, D., & Azar, A. T. (2015). Sliding modes for fault tolerant control. In A.T. Azar & Q Zhu (Eds.) *Advances and applications in sliding mode control systems, studies in computational intelligence book Series* (vol. 576, pp 407–433). Berlin: Springer GmbH. doi:10.1007/978-3-319-11173-5_15.

67. Luo, Y., & Chen, Y. (2012). Stabilizing and robust fractional order PI controller synthesis for first order plus time delay systems. *Automatica, 48*(9), 2159–2167.

68. Ebrahimkhani, S. (2016). *Robust fractional order sliding mode control of doubly-fed induction generator (dfig)-based wind turbines*. *ISA transactions*, 2016. In Press.
69. Munteanu, I., Bacha, S., Bratcu, A. I., Guiraud, J., & Roye, D. (2008). Energy-reliability optimization of wind energy conversion systems by sliding mode control. *IEEE Transactions on Energy Conversion, 23*(3), 975–985.
70. Beltran, B., Ahmed-Ali, T., & Benbouzid, M. E. H. (2008). Sliding mode power control of variable-speed wind energy conversion systems. *IEEE Transactions on Energy Conversion, 23*(2), 551–558.